

Investigation of Thruster Design to Obtain the Optimum Thrust for ROV (Remotely Operated Vehicle) Using CFD

Darmawan, Steven

Study Program of Mechanical Engineering, Faculty of Engineering, Universitas Tarumanagara

Raynaldo, Kevin

Study Program of Mechanical Engineering, Faculty of Engineering, Universitas Tarumanagara

Halim, Agus

Study Program of Mechanical Engineering, Faculty of Engineering, Universitas Tarumanagara

<https://doi.org/10.5109/4774224>

出版情報 : Evergreen. 9 (1), pp.115-125, 2022-03. Transdisciplinary Research and Education Center for Green Technologies, Kyushu University

バージョン :

権利関係 : Creative Commons Attribution-NonCommercial 4.0 International



Investigation of Thruster Design to Obtain the Optimum Thrust for ROV (Remotely Operated Vehicle) Using CFD

Steven Darmawan^{1,*}, Kevin Raynaldo^{1,2}, Agus Halim^{1,2}

¹Study Program of Mechanical Engineering, Faculty of Engineering, Universitas Tarumanagara, Jalan Letjen S. Parman No. 1, Jakarta Barat 11440, Indonesia

²PT. Matahari Megah, Jalan Raya Serang km 8.5 Kadu Jaya, Tangerang, Indonesia

*Author to whom correspondence should be addressed:

E-mail: stevend@ft.untar.ac.id

(Received February 11, 2022; Revised March 22, 2022; accepted March 22, 2022).

Abstract: Existing ROV (Remotely Operated Vehicle) requires optimization in thrust and maneuverability to compete in the next Robotic Event. Investigation to acquire optimum thrust by configuring its thruster is conducted. Variations of configurations consist of number of blades, propeller diameter, and application of kort nozzle. Furthermore, analysis is conducted using CFD (Computational Fluid Dynamics) approach with ANSYS CFX 2021 R1 for open water characteristics with Moving Reference Frame (MRF) method and SST k- ω for turbulent model. CFD results show that kort nozzle configuration is able to generate addition thrust by accelerating fluid flow through inner kort nozzle wall. The result denotes that thruster P3-2020 with kort nozzle obtains the optimum thrust in the amount of 0.0059 N which application of kort nozzle can increase the thrust by 2.253% and reduces turbulent flow distribution for 21.053%.

Keywords: ROV; Optimum Thrust; CFD; Thruster Configuration

1. Introduction

ROV (Remotely Operated Vehicle) is an underwater robot which is used to explore underwater photography, military operation, science needs, and rescue mission that is difficult to reach by human, such that it can replace human in doing underwater task¹⁻⁴). This ROV is being developed by Universitas Tarumanagara (UNTAR) Robotics Team to compete in the next Robotics Event. The previous competition in Robotics Event 2020 leads an innovation to improve the existing ROV during development process. Furthermore, some evaluations of ROV are conducted from preceding Robotics Event such as the need for optimization of thrust and improve its maneuverability. Both of these needs can be reached by investigation from propeller configuration as a part of thruster design with reference to existing propeller of ROV 2020^{1,2,5}). Thruster is powering prime mover or main locomotor component to maneuver horizontally when it moves forward and backward also vertically to move up and down^{1,3}). Thrust that produced by the thruster is one of the main performance parameters in ROV that enables better acceleration to achieve required speed and it is important in certain dynamic positioning situation^{6,7}). Better thrust operation of ROV can increase chance to obtain shorter time record which is need to win the competition.

Christ and Wernli consider that the main objective for ROV propulsion systems (propeller) design is to have

high thrust-to-physical size/drag and power-input ratios. ROV propeller will have better performance if the propeller produces higher thrust and power in lower revolution³). Then, Analysis for number of blades and application of kort nozzle with proper configuration is able to increase the thrust produced by propeller^{1,8}). Based on the problem, the thruster configuration for ROV is focused on number of blades and kort nozzle in order to improve existing performance of the ROV which does not present satisfying result in maneuverability yet.

Analysis to obtain the optimum thrust is conducted using CFD (Computational Fluid Dynamics) approach, so that pressure distribution phenomenon and fluid flow can be acquired^{1,2,5,9-13}). The CFD is also widely implemented in fluid flow analysis of aerodynamic performance^{14,15}), such as: to investigate the influence of active flow control of airfoil aerodynamic performance using OpenFOAM Solver^{16,17}), to observe movement of unmanned aerial vehicles (UAV) including lift and drag deployed for bird control using ANSYS Fluent¹⁸), and to optimize blended winglets configuration on Micro UAV according to airflow pattern, vortex structure, lift and drag using ANSYS Fluent¹⁹).

Besides, scope of the problem analyzed in this paper consists of thrust optimization which is restricted to number of blades (2, 3, and 4-blades) and application of kort nozzle. Furthermore, maximum propeller diameter is 40 mm to meet market availability and is set for 300 rpm.

Advance coefficient (J) for propeller operating condition at the competition is estimated by 0.473.

The objectives of the research are to optimize existing thruster design so it can produce optimum thrust and better maneuverability. The optimum thruster configuration result will be provided as a reference for UNTAR Robotics Team especially as thruster of ROV 2021 to compete in Robotics Event 2021.

2. Methodology

The research utilizes CAD software to design propeller while CFD software is used to conduct numerical computation. Then, existing thruster model of ROV 2020 of UNTAR Robotics Team can be shown in Fig. 1.

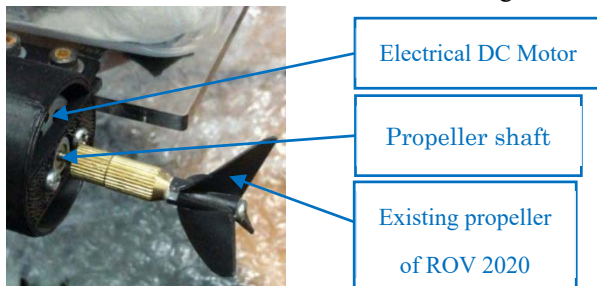


Fig. 1: Existing thruster model of ROV 2020

CFD simulation method is done using ANSYS CFX 2020 R1^{1,2,5,9,10,20,21}. The **Finish** for research method can be shown in

Fig. 2.

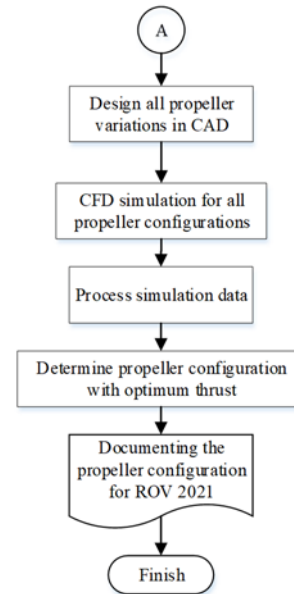
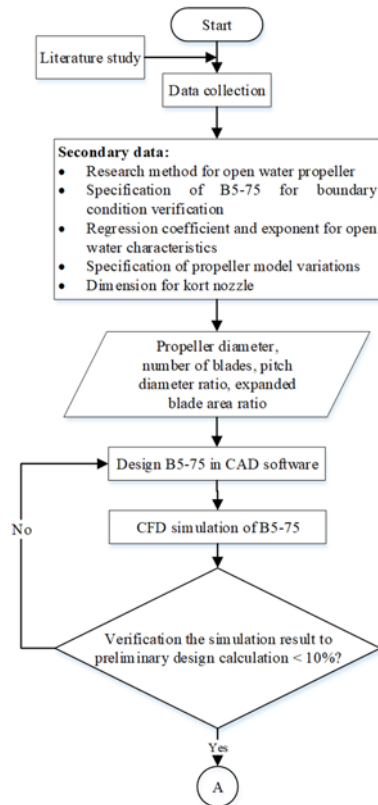


Fig. 2: Existing thruster model of ROV

2.1 CFD model

CFD model is conducted three dimensionally in this research with Moving Reference Frame (MRF) method^{1,2,6,21-24} which the boundary condition can be shown in Fig. 3.

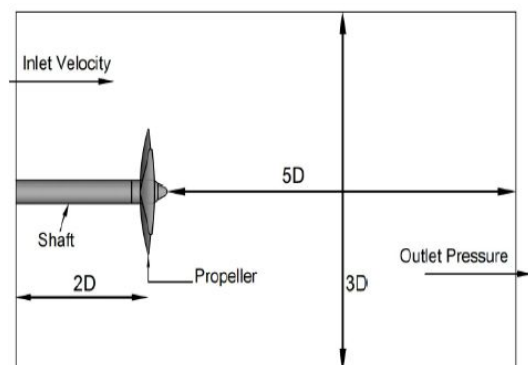


Fig. 3: Boundary condition of open water propeller^{1,2)}

There are two main domains in this MRF such as stationary domain and rotating domain. Stationary domain consists of fluid around the propeller analyzed while rotating domain consists of propeller which has smaller mesh than stationary domain^{6,22-25}. MRF utilizes frozen rotor concept in frame change/mixing for CFD modeling. Difference in mesh size is intended to obtain better computation although it needs longer time²⁶. Furthermore, turbulent analysis is conducted using shear stress transport (SST) $k-\omega$ ^{6,22,25}. The SST $k-\omega$ of Menter's model is used in ANSYS CFX which the Reynolds stress computation and the k -equation are the same as in Wilcox's original $k-\omega$ model. However, ε -equation is transformed into an ω -equation by substituting $\varepsilon = k\omega$ ²⁰. The SST $k-\omega$ turbulent model approach is employed in the sublayer of the boundary layer. It improves the accuracy of prediction of

flows phenomenon for pressure-induced boundary layer separation²⁷). Therefore, this turbulent model is suitable to be applied in simulation of propeller configuration which is focused on calculation at boundary layer, such as interface between blade-water and kort nozzle-wall at high Reynolds number. Furthermore, SST $k-\omega$ has better accuracy to analyze and to represent flows phenomenon near kort nozzle, especially swirl flow which is probably occurred after the fluid flows through kort nozzle. On the other hand, airfoil approach can be considered for calculating the Reynolds number (Re) when the fluid flows through kort nozzle profile which has variables such as reference length (L), reference fluid velocity (v), fluid density (ρ) and fluid viscosity (μ)²⁸. In example, kort nozzle for existing propeller 3-blades ROV 2020 will have reference length for 25.9 mm; the fluid velocity is estimated by 0.2 m/s; the fluid density is set by 998.2 kg/m³; and the fluid viscosity is set by 8.53×10^{-4} Ns/m²; hence the Reynolds number of the flowing fluid through kort nozzle is 6,061.754.

Equation of Menter SST $k-\omega$ model consist of the transport equations for the turbulent kinetic energy and the specific dissipation of turbulent which can be expressed in equation (1) and (2), respectively²⁸.

$$\begin{aligned} & \text{(I)} \quad \text{(II)} \quad \text{(III)} \\ & \frac{\partial \rho K}{\partial t} + \frac{\partial}{\partial x_j} (\rho v_j K) = \frac{\partial}{\partial x_j} \left[(\mu L + \sigma K \mu T) \frac{\partial K}{\partial x_j} \right] \quad (1) \\ & + \tau_{ij}^F S_{ij} - \beta^* \rho \omega K \quad \text{(IV)} \quad \text{(V)} \end{aligned}$$

The equation (1) consists of five terms: term (I) is rate of change of K ; term (II) is transport of K by convection; term (III) is transport of K by turbulent diffusion; term (IV) is Favre-averaged turbulent stresses and the strain rate tensor; term (V) is rate of dissipation of K ^{20,28}.

$$\begin{aligned} & \text{(I)} \quad \text{(II)} \quad \text{(III)} \\ & \frac{\partial \rho \omega}{\partial t} + \frac{\partial}{\partial x_j} (\rho v_j \omega) = \frac{\partial}{\partial x_j} \left[(\mu L + \sigma_\omega \mu T) \frac{\partial \omega}{\partial x_j} \right] \quad (2) \\ & + \frac{C_\omega \rho}{\mu T} \tau_{ij}^F S_{ij} - \beta \rho \omega^2 + 2(1 - f_1) \frac{\rho \sigma_{\omega 2}}{\omega} \frac{\partial K}{\partial x_j} \frac{\partial \omega}{\partial x_j} \quad \text{(IV)} \quad \text{(V)} \quad \text{(VI)} \end{aligned}$$

The equation (2) consists of six terms: term (I) is rate of change of ω ; term (II) is transport of ω by convection; term (III) is transport of ω by turbulent diffusion; term (IV) is Eddy-viscosity production; term (V) is the rate of dissipation of ω ; and term (VI) is the cross-diffusion terms^{20,28}.

2.2 Verification of Boundary Condition

Verification of boundary condition is conducted using preliminary design calculation to estimate the thrust produced and required torque with a sample B-series propeller (B5-75) that is obtained from another researcher¹). The preliminary design calculation can be applied for propeller with B-series outline at Reynolds number (Re) $< 2 \times 10^6$ only^{29,30}. If the sample B5-75 is verified, the same boundary condition can be applied for all propeller configurations model.

The verification for B5-75 utilizes some parameters such as 5-blades for number of blades (z); 0.75 for expanded blade area ratio; 0.6 for pitch diameter ratio; and 0.15 is assumed as value of J ¹). Furthermore, propeller revolution will be set in the range of 100; 200; 300; 400 and 500 rpm. The preliminary design calculation employs thrust coefficient (K_T) and torque coefficient (K_Q) as function of number of blade (Z), expanded blade area ratio (A_E/A_0), pitch diameter ratio (P/D) and advance coefficient as shown in equation (3) and (4) respectively^{1,2,29,30}.

$$K_T = \sum_{n=1}^{39} (C_{Tn}) (J^{S_n}) \left(\frac{P}{D} \right)^{t_n} \left(\frac{A_E}{A_0} \right)^{U_n} (Z^{v_n}) \quad (3)$$

$$K_Q = \sum_{n=1}^{47} (C_{Qn}) (J^{S_n}) \left(\frac{P}{D} \right)^{t_n} \left(\frac{A_E}{A_0} \right)^{U_n} (Z^{v_n}) \quad (4)$$

Where C_{Tn} and C_{Qn} are the regression coefficients of the thrust and torque coefficients respectively, while S_n , t_n , U_n and v_n are the exponents of J , P/D , A_E/A_0 , and Z respectively. The value for the regression coefficients and exponent of K_T - K_Q at equation (3) and (4) are given in ²⁹.

Then, the value of K_T and K_Q that are obtained from equation (3) and (4) will be substituted to equation (5) and (6) to get thrust produced (T) in N and required torque (Q) in Nm^{1,2,29,30}.

$$T = K_T (\rho n^2 D^4) \quad (5)$$

$$Q = K_Q (\rho n^2 D^5) \quad (6)$$


Where ρ is fluid density (kg/m³), n is revolution (rps) and D is propeller diameter (m).

Furthermore, this research can be used as reference to compare experimental data to simulation result in order to create interrelated data³¹.

2.3 Existing ROV design

Existing ROV design competed in Robotics Event 2020 and its specification can be shown Table 1. The existing ROV will be developed by implementing the best thruster configuration.

Table 1: Existing specification of ROV 2020

	P3-2020	
	Dimension	Value
	Total mass in air	1,5 kg
	Total weight in air	14,715 N

2.4 Existing propeller design

Existing propeller configuration used in ROV 2020 is named as propeller 3-blade ROV 2020 or abbreviated as P3-2020. The specification of P3-2020 can be shown in エラー! 参照元が見つかりません。 Furthermore, there are 8 thruster configurations to be considered for ROV 2021. They are P3-2020 with and without kort nozzle; new 2-blades propeller (abbreviated as P2-New) with and without kort nozzle; new 3-blades propeller (abbreviated as P3-New) with and without kort nozzle and new 4-blades propeller (abbreviated as P4-New) with and without kort nozzle. The kort nozzle used for thruster configuration is based on Shuskin nozzle type-C which clearance between blade tip and inside kort nozzle wall is set by 1% from propeller diameter ^{22,32}).

Table 2: Specification of P3-2020


	P3-2020	
	Specification	Value
	Pitch diameter ratio	1.4
	Blade diameter	35 mm
	Expanded blade area ratio	0.511
	Outline	Custom

Table 3: Specification of new propeller configuration as comparison

P2-New	
Specification	Value
Pitch diameter ratio	1.4
Blade diameter	30 mm
Expanded blade area ratio	0.327
Outline	Custom

P3-New	
Specification	Value
Pitch diameter ratio	1.4
Blade diameter	32 mm
Expanded blade area ratio	0.703
Outline	Custom
P4-New	
Specification	Value
Pitch diameter ratio	1.4
Blade diameter	40 mm
Expanded blade area ratio	0.75
Outline	BB-series

2.5 Computational mesh

Computational mesh used in the CFD simulation both rotating domain and stationary domain is general mesh or unstructured mesh arrangements. The computational mesh of all thruster configurations can be shown in Fig. 4 until Fig. 11.

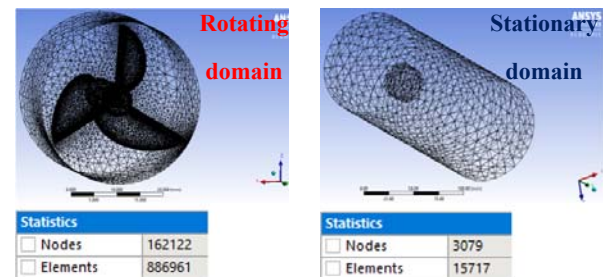


Fig. 4: Computational mesh of P3-2020

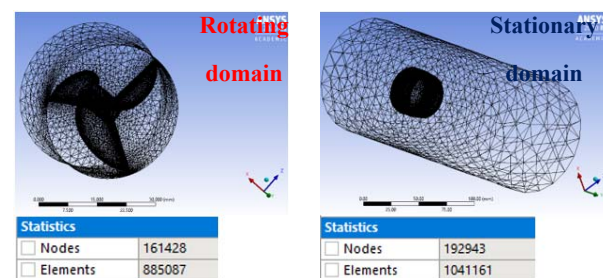


Fig. 5: Computational mesh of P3-2020 with kort nozzle

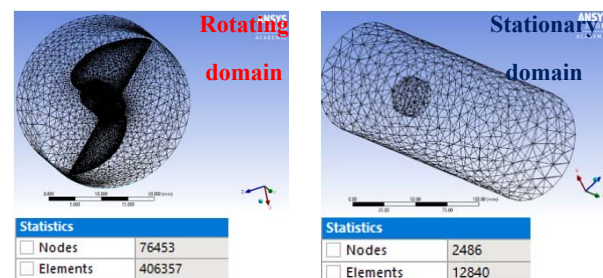


Fig. 6: Computational mesh of P2-New

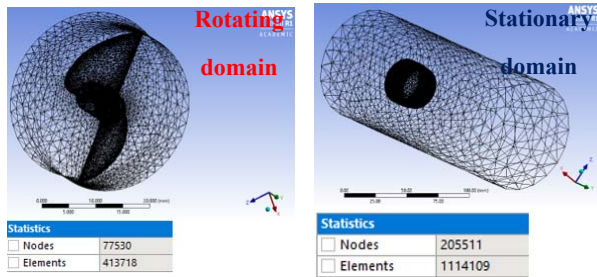


Fig. 7: Computational mesh of P2-New with kort nozzle

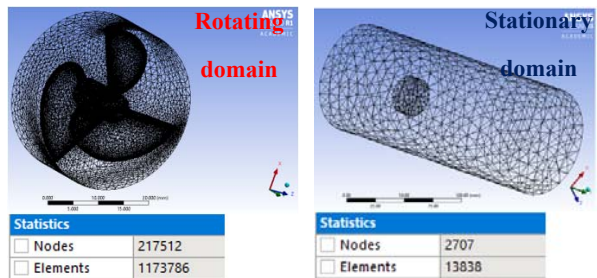


Fig. 8: Computational mesh of P3-New

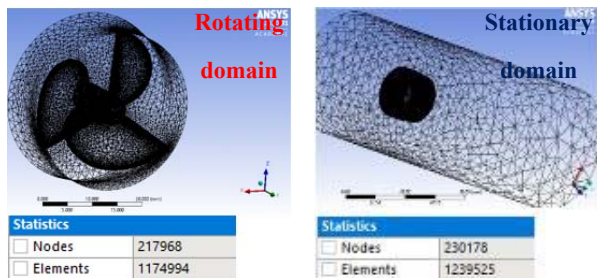


Fig. 9: Computational mesh of P3-New with kort nozzle

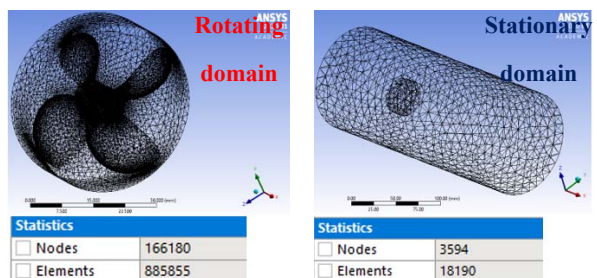


Fig. 10: Computational mesh of P4-New

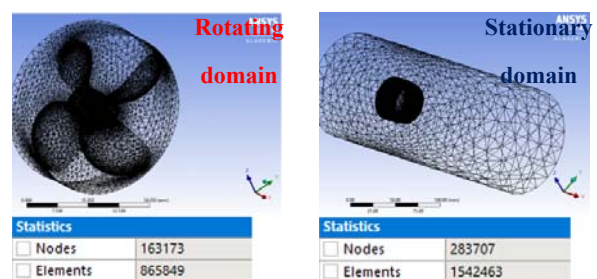


Fig. 11: Computational mesh of P4-New with kort nozzle

2.6 Set up dan solution

Domains and boundary conditions will be set up in the CFX-Pre which implementation of them into propeller simulation are according to “エー! 参照元が見つかり

ません。” Subsection. The fluid material for stationary and rotating domain are set as water at 25 °C and 1 atm reference pressure. In the rotating domain, there is determination of propeller angular velocity. Then, boundary conditions set up consider two main elements such as inlet and outlet. Velocity inlet takes into account for inlet boundary condition. On the other side, relative outlet pressure represented the depth of propeller is considered as outlet boundary condition. The setting up of CFX-Pre can be seen in Fig. 12.

Furthermore, computation process utilizes ASUS LAPTOP-LSD39VTN which the specifications are as follows: Windows 10 Home 64-bit Operating System, Intel(R) Core (TM) i7-8550U processor and 8 GB RAM. Then, solution is done using CFX Solver Manager which is available in Fig. 13.

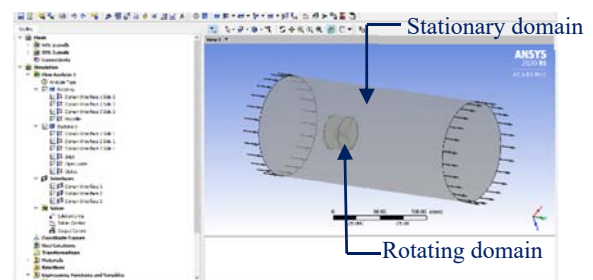


Fig. 12: CFX-Pre

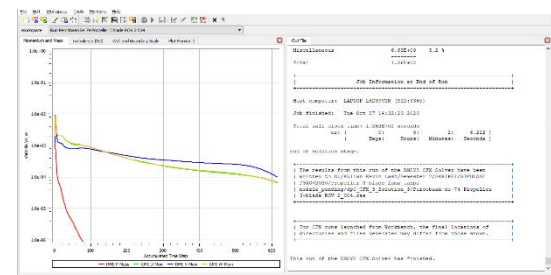


Fig. 13: CFX solver manager

3. Result and discussion

3.1 Verification for sample B5-75

Verification process of boundary condition is based on thrust verification only. Then, thrust verification result for CFD simulation of sample propeller B5-75 to preliminary design calculation (calculated from equation (5)) can be shown in Table 4. The CFD simulation results in thrust is in accordance with equation 5 and can be applied on torque calculation on equation 6. Both preliminary design and CFD simulation show that addition in revolution leads increasing in thrust produced by propeller.

Table 4: Thrust verification result between CFD simulation to preliminary design calculation

Revolution	Thrust of Preliminary Design Calculation	Thrust of CFD Simulation	Absolute Deviation
100 rpm	0,17 N	0,151 N	11,176%
200 rpm	0,68 N	0,625 N	8,088%
300 rpm	1,529 N	1,419 N	7,194%
400 rpm	2,717 N	2,554 N	5,999%
500 rpm	4,244 N	4,01 N	5,514%

Absolute deviation between CFD simulation to preliminary design calculation which can be accepted is lower than 10% ($< 10\%$). Based on Table, the absolute deviation from 200 rpm to 500 rpm is lower than 10% so this value can be accepted. However, the absolute deviation at 100 rpm is higher than 10% and it cannot be accepted. This phenomenon shows that there is limitation for propeller revolution to be verified. On the other hand, this verification is only consideration for understanding that the boundary condition and CFD modeling is already confirmed. Furthermore, the revolution of all thruster configurations is set by 300 rpm, so the similar boundary condition and CFD modeling can be applied to discover optimum thrust.

3.2 CFD result of thruster configurations

CFD simulation of all thruster configurations is at 300 rpm and $J = 0.473$ as operating condition of propeller which can be shown in Fig. 14 until Fig. 21.

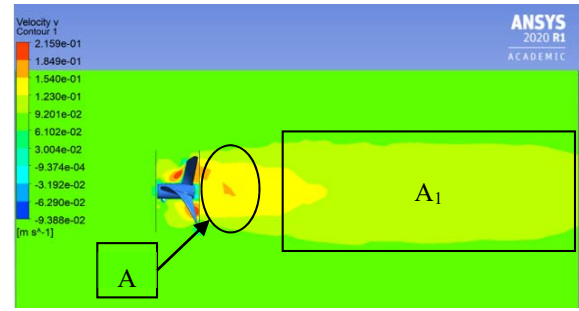
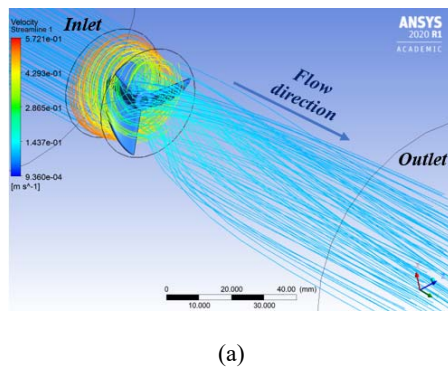


Fig. 14: CFD simulation for P3-2020: (a) Velocity streamline; (b) Velocity v contour

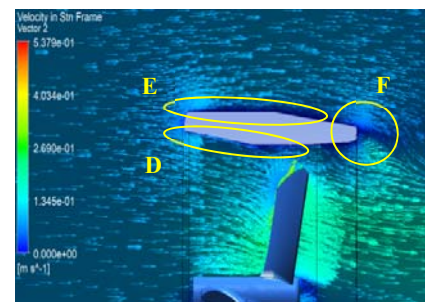
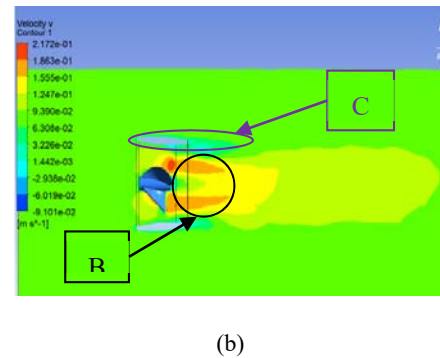
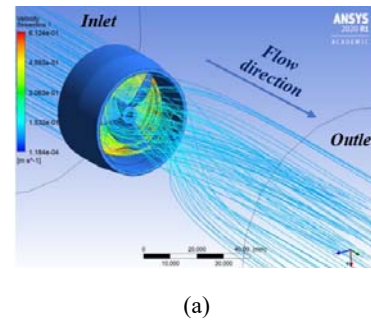
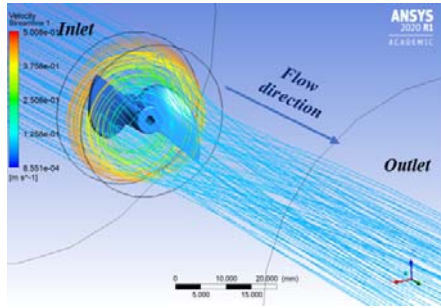
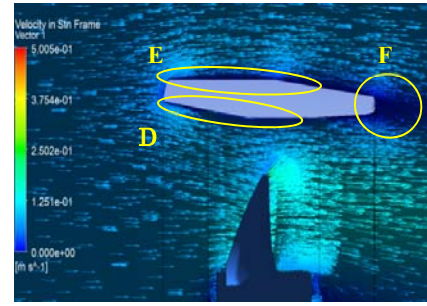


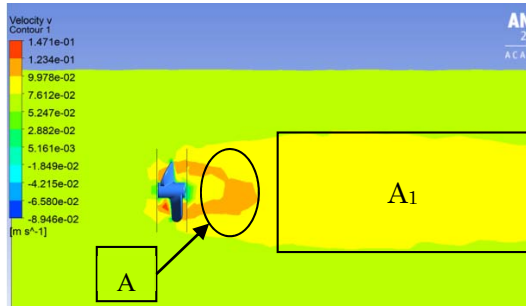
Fig. 15: CFD simulation for P3-2020 with Kort nozzle: (a) Velocity streamline; (b) Velocity v contour; (c) Velocity in stn frame vector



(a)

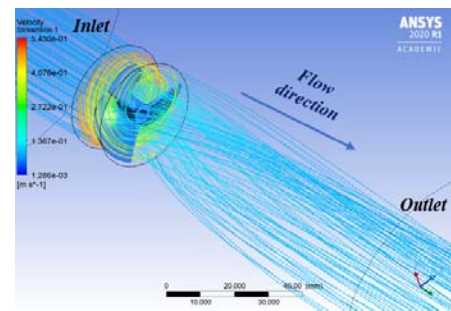


(c)

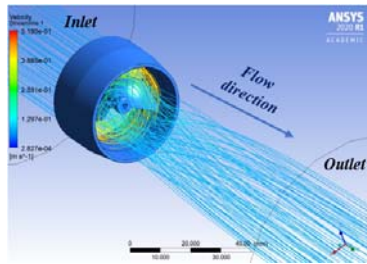


(b)

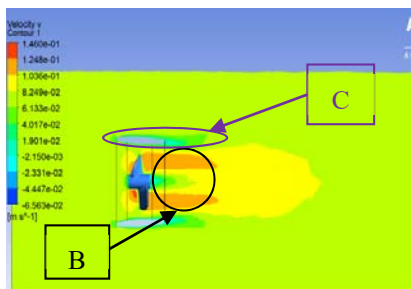
Fig. 16: CFD simulation for P2-New: (a) Velocity streamline; (b) Velocity v contour



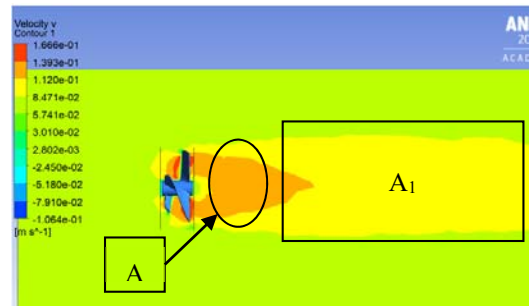
(a)



(a)

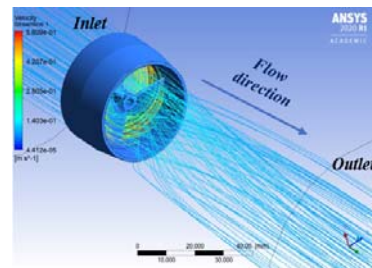


(b)

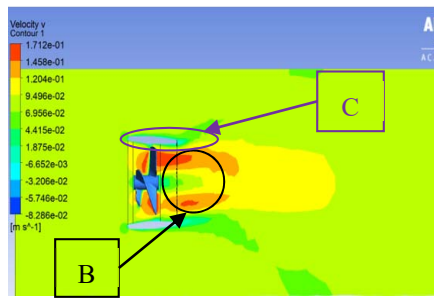


(b)

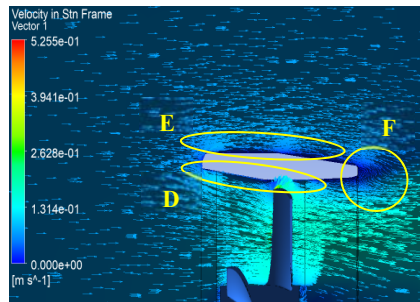
Fig. 18: CFD simulation for P3-New: (a) Velocity streamline; (b) Velocity v contour



(a)

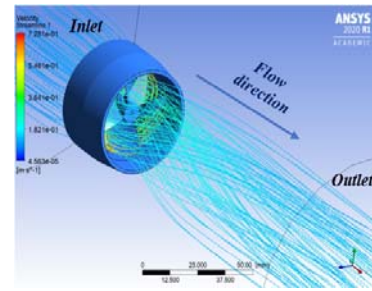


(b)

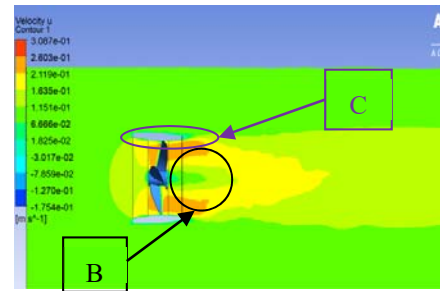


(c)

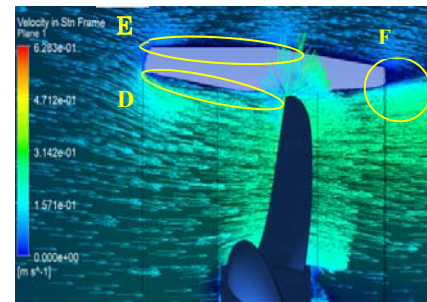
Fig. 19: CFD simulation for P3-New with kurt nozzle: (a) Velocity streamline; (b) Velocity v contour; (c) Velocity in stn frame vector



(a)

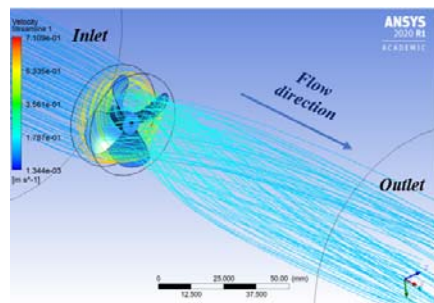


(b)

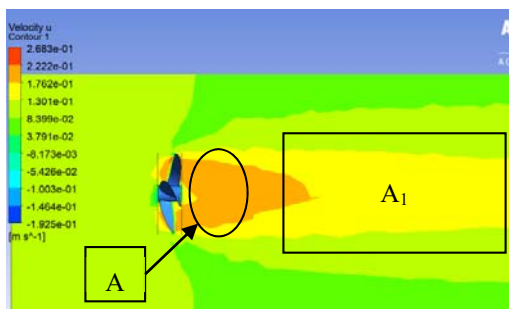


(c)

Fig. 21: CFD simulation for P4-New with kurt nozzle: (a) Velocity streamline; (b) Velocity u contour; (c) Velocity in stn frame vector



(a)



(b)

Fig. 20: CFD simulation for P4-New: (a) Velocity streamline; (b) Velocity u contour

CFD simulation results can be represented by velocity contour such as configuration without kurt nozzle as shown in Fig. 14(b); Fig. 16(b); Fig. 18(b) and Fig. 20(b) which have area A and they represent thrust distribution in term of fluid velocity escalation in the range of 0.0998 m/s – 0.222 m/s. Then, the distribution of velocity around the propeller decreased along the outlet in the range of 0.0761 m/s – 0.13 m/s which flow phenomenon can be seen in area A₁. On the other hand, simulation results of velocity contour for configuration with kurt nozzle are available in Fig. 15(b); Fig. 17(b); Fig. 19(b) and Fig. 21(b) that have area B and C as analysis points. B represents thrust produced by propeller in term of fluid velocity concentration in the range of 0.104 m/s – 0.26 m/s, while C represents thrust produced by kurt nozzle in term of fluid velocity in the range of 0.00215 m/s – 0.0667 m/s. Kurt nozzle configuration has total thrust which is addition of thrust produced by propeller and thrust produced by kurt nozzle as formulated by ²⁴). In general, it enables configuration with kurt nozzle having better thrust than without kurt

nozzle as in example: P3-2020 with kort nozzle (Fig. 15 (b)) has 0.16 m/s velocity after flowing through kort nozzle at B and 0.03 m/s velocity at C which the total velocity is higher than P3-2020 without kort nozzle (Fig. 14(b)). P3-2020 has 0.13 m/s velocity at A and it has turbulent flow distribution of 0.12 m/s at A₁. Furthermore, application of kort nozzle has chance to increase thrust produced by propeller through concentration and acceleration of fluid flow after passing kort nozzle. Then, kort nozzle can reduce the turbulent flow distribution that is caused by propeller revolution.

Application of kort nozzle leads some influences to fluid flow around its hydrodynamic profile. Based on Fig. 15(c); Fig. 17(c); Fig. 19(c) and Fig. 21(c), there is acceleration of fluid flow through inner kort nozzle wall that is appointed by faster flow velocity vector than outer side. Those figures show that every thruster configuration have the same fluid flow characteristics along area D, E and F which are marked by yellow circle. Area D represents fluid flow phenomenon near inner wall while area E represents fluid flow phenomenon near outer side. Then, Area F is fluid flow phenomenon which is influenced by different characteristic in area D and E. Furthermore, the velocity vector in area D is faster than area E; in example P3-2020 with kort nozzle has 0.15 m/s velocity at D while area E has 0.09 m/s velocity. It means that pressure along streamline D is lower than streamline E. Then, pressure difference between area D and E leads minor swirling where is represented by area F. The swirling vector begins from higher pressure of streamline E to lower pressure of streamline D. Nevertheless, this minor swirling has no significant impact to thruster's performance.

Hydrodynamic profile of kort nozzle enables acceleration of fluid flow because of cross sectional area difference between inlet-kort nozzle and outlet-kort nozzle. The increasing velocity of fluid flow in area D denotes increasing fluid particles momentum towards propeller, so higher momentum in the same time will increase the thrust that is produced by propeller. This phenomenon is appropriate with Newton's second law.

Furthermore, the thrust comparison of all thruster configurations at 300 rpm can be shown in Fig. 22 which are proceed in post-CFD. Thrust calculation process for thruster configurations use function calculator in post-CFD.

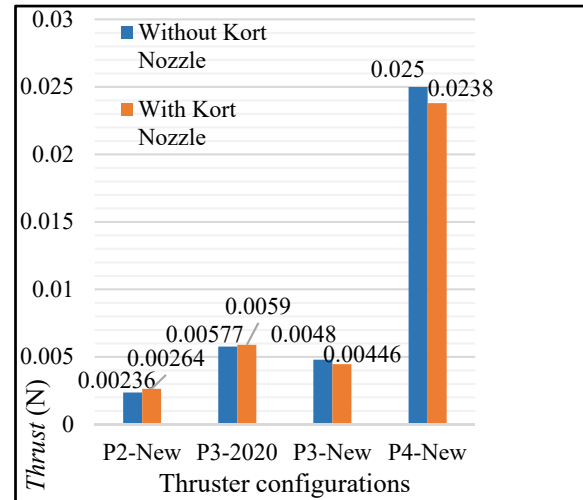


Fig. 22: Thrust produced from post-CFD at 300 rpm

Table 5: Thrust comparison of thruster configuration at 300 rpm

No.	Thrust Configurations	Thrust (N)		Thrust Change (%)
		without kort nozzle	with kort nozzle	
1	P2-New	0.00236	0.00264	+11.864
2	P3-2020	0.00577	0.0059	+2.253
3	P3-New	0.0048	0.00446	-7.083
4	P4-New	0.025	0.0238	-4.8

Based on Fig. 22 and Table 5, application of kort nozzle for P2-New and P3-2020 are successful to increase thrust produced by 11.864% and 2.253% respectively. However, these increasing of thrust are not satisfied yet because of the propeller optimum operating condition does not be achieved yet. Investigation to obtain optimum operating condition for propeller will be done in further research. On the other hand, decreasing of thrust on P3-New and P4-New in the amount of 7.083% and 4.8% respectively is also caused of optimum operating condition does not be achieved yet.

The result shows that there is tendency in increasing of thrust to number of blade and propeller diameter. P2-New without kort nozzle has the lowest thrust produced with 0.00236 N. The highest thrust achieved from all configurations is P4-New without kort nozzle with 0.025 N. This configuration is not chosen because it is only thruster comparison and is not available on market and is also complicated for manufacturing. However, P4-New is still hoped to be developed in the future due to the performance. At present, it is only used to describe how number of blades and diameter influences the thrust generated.

Based on the condition, P3-2020 with kort nozzle for the second highest thrust with 0.0059 N is chosen to be recommended for UNTAR Robotics Team as thruster of ROV 2021. This configuration with kort nozzle also

reduces the turbulent that is caused by rotating propeller especially around the blade tip to ROV body which is stated by comparison in Fig. 23. The comparison is conducted using constant scale gridlines approach to gain total turbulent flow distribution reduction of application of P3-2020 with kort nozzle. Total vertical grid for configuration without kort nozzle is 19 grids, while configuration with kort nozzle is 15 grids and so the total turbulent flow reduction of configuration with kort nozzle is 21.053%.

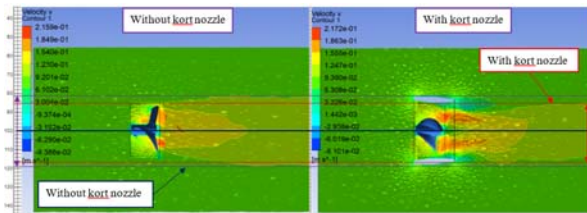


Fig. 23: Turbulent flow comparison of P3-2020 configuration

Total reduction of turbulent flow distribution of P3-2020 with kort nozzle has better chance to improve ROV maneuverability that is appropriate for competition. The kort nozzle wall bounds the flow and may provide the increasing flow intensity near wall and leaving the propeller.

4. Conclusion

CFD simulation results for all thruster configurations show that there is tendency in increasing of thrust produced to number of blade and propeller diameter. Increasing either the number of blade and propeller diameter in optimum amount will produce higher thrust. Then, application of kort nozzle to propeller can produce more thrust in appropriate operating condition. P3-2020 with kort nozzle is the best thruster configuration achieved with optimum thrust that will be recommended to UNTAR Robotics Team for ROV 2021. This thruster utilizes with kort nozzle and is able to increase the thrust by 2.253%, so the total thrust becomes 0.0059 N. Furthermore, the recommended thruster can reduce the turbulent flow distribution for 21.053% and so it has better chance to increase the ROV stability and maneuverability.

5. Future work

Thruster design P4-New is very potential to be implemented once the manufacturing method is suitable to the thruster P4-New design requirement. Adjustment or compliance between mechanical design and manufacturing process may be needed for supporting the development in future research.

Acknowledgements

Author would like to thank you for Study Program of Mechanical Engineering of Universitas Tarumanagara and

PT. Matahari Megah as Engineering-based Company for supporting this research.

Nomenclature

J	advance coefficient (–)
Re	Reynolds number (–)
L	reference length (m)
v	reference fluid velocity (m/s)
ρ	fluid density (kg/m ³)
μ	fluid dynamic viscosity (Ns/m ²)
K_T	thrust coefficient (–)
K_Q	torque coefficient (–)
Z	number of blades (unit)
A_E/A_0	expanded blade area ratio (–)
P/D	pitch diameter ratio (–)
C_{Tn}	regression coefficient of thrust (–)
C_{Qn}	regression coefficient of torque (–)
S_n	exponent of J (–)
t_n	exponent of P/D (–)
U_n	exponent of A_E/A_0 (–)
v_n	exponent of Z (–)
n	propeller revolution (rps)
D	propeller diameter (m)

References

- 1) A. Bahatmaka, D.-J. Kim, and D. Chrismianto, "Optimization of ducted propeller design for the rov (remotely operated vehicle) using cfd," *Adv. Technol. Innov.*, **2** (3) 73–84 (2016).
- 2) A. Bahatmaka, D.J. Kim, D. Chrismianto, N. Hai, and A.R. Prabowo, "Optimization of thrust propeller design for an ROV (Remotely Operated Vehicle) consideration by Genetic Algorithms," in: MATEC Web Conf., 2017. doi:10.1051/mateconf/201713807003.
- 3) R.D. Christ, and R.L. Wernli, "The ROV Manual: A User Guide for Remotely Operated Vehicles: Second Edition," 2013. doi:10.1016/C2011-0-07796-7.
- 4) F.N. Zohedi, M.S. Mohd Aras, H.A. Kasdirin, and M.B. Bahar, "A new tuning approach of single input fuzzy logic controller (siflc) for remotely operated vehicle (rov) depth control," *Evergreen*, **8** (3) (2021). doi:10.5109/4491657.
- 5) Z. Abidin, D. Chrismianto, and A. Trimulyono, "Analisa underwater thruster pada remotely operated vehicle (rov) dengan metode cfd [analysis of underwater thruster of remotely operated vehicle (rov) using cfd method]," *J. Tek. Perkapalan*, **3** (2) (2015).
- 6) T.H. Joung, H.S. Choi, S.K. Jung, K. Sammut, and F. He, "Verification of cfd analysis methods for predicting the drag force and thrust power of an underwater disk robot," *Int. J. Nav. Archit. Ocean*

- Eng.*, **6** (2) 269–281 (2014). doi:10.2478/IJNAOE-2013-0178.
- 7) J. Carlton, “Marine Propellers and Propulsion: Fourth Edition,” Butterworth-Heinemann, 2019.
 - 8) D. Gerr, “Propeller Handbook: The Complete Reference for Choosing, Installing, and Understanding Boat Propellers,” McGraw-Hill Professional, 2001.
 - 9) Y. cun Pan, H. xin Zhang, and Q. dou Zhou, “Numerical simulation of unsteady propeller force for a submarine in straight ahead sailing and steady diving maneuver,” *Int. J. Nav. Archit. Ocean Eng.*, **11** (2) 899–913 (2019). doi:10.1016/j.ijnaoe.2019.04.002.
 - 10) D.A.D. Rahman, “Studi Kasus Modifikasi Daun Propeller Pada MV. Meratus Barito,” Institut Teknologi Sepuluh Nopember, 2016. <http://repository.its.ac.id/51141/>.
 - 11) I.S. Arief, T.B. Musriyadi, and A.D.A. Je Mafera, “Analysis effect of duct length– nozzle diameter ratio and tip clearance variation on the performance of k-series propeller,” *Int. J. Mar. Eng. Innov. Res.*, **2** (1) (2017). doi:10.12962/j25481479.v2i1.2527.
 - 12) K. Muljowidodo, S. Adi N., A. Budiyo, and N. Prayogo, “Design of shrimp roe for surveillance and mine sweeper,” *Indian J. Mar. Sci.*, **38** (3) 332–337 (2009).
 - 13) S. Subhas, V.F. Saji, S. Ramakrishna, and H.N. Das, “CFD analysis of a propeller flow and cavitation,” *Int. J. Comput. Appl. Technol.*, **55** (16) 26–33 (2012). doi:10.5120/8841-3125.
 - 14) N.I. Ismail, H. Sharudin, M.M. Mahadzir, Z.M. Ali, A.A. Shariffuddin, and N.I. Kamel, “Computational aerodynamics study on neo-pto micro unmanned aerial vehicle,” *Evergreen*, **8** (2) (2021). doi:10.5109/4480726.
 - 15) M.M. Takeyeldein, T.M. Lazim, N.A.R. Nik Mohd, I.S. Ishak, and E.A. Ali, “Wind turbine design using thin airfoil sd2030,” *Evergreen*, **6** (2) (2019). doi:10.5109/2321003.
 - 16) A.M. Halawa, B. Elhadidi, and S. Yoshida, “Aerodynamic performance enhancement using active flow control on du96-w-180 wind turbine airfoil,” *Evergreen*, **5** (1) (2018). doi:10.5109/1929723.
 - 17) A.M. Halawa, B. Elhadidi, and S. Yoshida, “POD & mslm application on du96-w180 wind turbine airfoil,” *Evergreen*, **4** (1) (2017). doi:10.5109/1808451.
 - 18) S. Ibrahim, B. Alkali, A. Oyewole, S.B. Alhaji, A.A. Abdullahi, and G. Ibrahim Aku, “Structural integrity study for a quadcopter frame to be deployed for pest control,” *Evergreen*, **8** (3) (2021). doi:10.5109/4491843.
 - 19) D. Danardono, D. Prija, I. Yaningsih, B. Yansa, L. Imama, and A.R. Prabowo, “Aerodynamic performance enhancement of wing body micro uav employing blended winglet configuration,” *J. Nov. Carbon Resour. Sci. Green Asia Strateg.*, **08** (04) 0 (2021).
 - 20) H.K. Versteeg, and W. Malalasekera, “Computational Fluid Dynamics: The Finite Volume Method,” 2nd ed., 2007. http://books.google.nl/books?id=RvBZ-UMpGzIC&hl=nl&source=gbbs_navlinks_s.
 - 21) L. Yu, M. Greve, M. Druckenbrod, and M. Abdel-Maksoud, “Numerical analysis of ducted propeller performance under open water test condition,” *J. Mar. Sci. Technol.*, **18** (3) 381–394 (2013). doi:10.1007/s00773-013-0215-4.
 - 22) S. Majdfar, H. Ghassemi, H. Forouzan, and A. Ashrafi, “Hydrodynamic prediction of the ducted propeller by cfd solver,” *J. Mar. Sci. Technol.*, **25** (3) 268–275 (2017). doi:10.6119/JMST-016-1214-2.
 - 23) M. Voerman, “Research into the effect of Counter-Rotating Propellers, for the propulsion of a Vertical Take-Off and Landing Ducted Fan UAV, n the flow pattern,” 2012.
 - 24) Q. Zhang, R.K. Jaiman, P. Ma, and J. Liu, “Investigation on the performance of a ducted propeller in oblique flow,” *J. Offshore Mech. Arct. Eng.*, **142** (1) (2020). doi:10.1115/1.4043943.
 - 25) M. Stajuda, M. Karczewski, D. Obidowski, and K. Jóźwik, “Development of a cfd model for propeller simulation,” *Mech. Mech. Eng.*, **20** (4) 579–593 (2016).
 - 26) S. Darmawan, and H. Tanujaya, “CFD investigation of flow over a backward-facing step using an rng k-ε turbulence model,” *Int. J. Technol.*, **10** (2) 280–289 (2019). doi:10.14716/ijtech.v10i2.800.
 - 27) J. Blazek, “Computational Fluid Dynamics: Principles and Applications,” 2005. doi:10.1016/B978-0-08-044506-9.X5000-0.
 - 28) S. Gudmundsson, “The Anatomy of the Airfoil,” in: *Gen. Aviat. Aircr. Des.*, 2014: pp. 235–297. doi:10.1016/b978-0-12-397308-5.00008-8.
 - 29) M.W.C. Oosterveld, and P. van Oossanen, “Further computer-analyzed dat of the wageningen b-screw series,” *Int. Shipbuild. Prog.*, **22** (251) 251–262 (1975). doi:10.3233/isp-1975-2225102.
 - 30) M.M. Gaafary, H.S. El-Kilani, and M.M. Moustafa, “Optimum design of b-series marine propellers,” *Alexandria Eng. J.*, **50** (1) 13–18 (2011). doi:10.1016/j.aej.2011.01.001.
 - 31) A.P. Irawan, A. Halim, and H. K., “Hybrid robot system design,” *IOP Conf. Ser. Mater. Sci. Eng.* **237** 012006, (2017).
 - 32) H. Schneekluth, and V. Bertram, “Ship Design for Efficiency and Economy,” Butterworth Heinemann, 1998. doi:10.1016/b978-0-7506-4133-3.x5000-2.